

## ORIGINAL RESEARCH

# Biallelic loss-of-function *ZFYVE19* mutations are associated with congenital hepatic fibrosis, sclerosing cholangiopathy and high-GGT cholestasis

Weisha Luan <sup>1,2</sup>, Chen-Zhi Hao,<sup>2</sup> Jia-Qi Li,<sup>1,2</sup> Qing Wei,<sup>3</sup> Jing-Yu Gong,<sup>1</sup> Yi-Ling Qiu <sup>1,2</sup>, Yi Lu,<sup>2</sup> Cong-Huan Shen,<sup>4</sup> Qiang Xia,<sup>5</sup> Xin-Bao Xie,<sup>2</sup> Mei-Hong Zhang,<sup>1</sup> Kuerbanjiang Abuduxikuer <sup>2</sup>, Zhong-Die Li,<sup>2</sup> Li Wang,<sup>2</sup> Qing-He Xing,<sup>6</sup> A S Knisely,<sup>7</sup> Jian-She Wang<sup>2</sup>

► Additional material is published online only. To view, please visit the journal online (<http://dx.doi.org/10.1136/jmedgenet-2019-106706>).

For numbered affiliations see end of article.

## Correspondence to

Dr Jian-She Wang, The Center for Pediatric Liver Diseases, Children's Hospital, Fudan University, Shanghai, Shanghai, China; [jshwang@shmu.edu.cn](mailto:jshwang@shmu.edu.cn)

WL, C-ZH and J-QL contributed equally.

Received 17 November 2019  
Revised 28 May 2020  
Accepted 20 June 2020



© Author(s) (or their employer(s)) 2020. No commercial re-use. See rights and permissions. Published by BMJ.

**To cite:** Luan W, Hao C-Z, Li J-Q, et al. *J Med Genet* Epub ahead of print: [please include Day Month Year]. doi:10.1136/jmedgenet-2019-106706

## ABSTRACT

**Background** For many children with intrahepatic cholestasis and high-serum gamma-glutamyl transferase (GGT) activity, a genetic aetiology of hepatobiliary disease remains undefined. We sought to identify novel genes mutated in children with idiopathic high-GGT intrahepatic cholestasis, with clinical, histopathological and functional correlations.

**Methods** We assembled a cohort of 25 children with undiagnosed high-GGT cholestasis and without clinical features of biliary-tract infection or radiological features of choledochal malformation, sclerosing cholangitis or cholelithiasis. Mutations were identified through whole-exome sequencing and targeted Sanger sequencing. We reviewed histopathological findings and assessed phenotypical effects of *ZFYVE19* deficiency in cultured cells by immunofluorescence microscopy.

**Results** Nine Han Chinese children harboured biallelic, predictedly complete loss-of-function pathogenic mutations in *ZFYVE19* (c.314C>G, p.S105X; c.379C>T, p.Q127X; c.514C>T, p.R172X; c.547C>T, p.R183X; c.226A>G, p.M76V). All had portal hypertension and, at liver biopsy, histopathological features of the ductal plate malformation (DPM)/congenital hepatic fibrosis (CHF). Four children required liver transplantation for recurrent gastrointestinal haemorrhage. DPM/CHF was confirmed at hepatectomy, with sclerosing small-duct cholangitis. Immunostaining for two primary-cilium axonemal proteins found expression that was deficient intraluminally and ectopic within cholangiocyte cytoplasm. *ZFYVE19* depletion in cultured cells yielded abnormalities of centriole and axoneme.

**Conclusion** Biallelic *ZFYVE19* mutations can lead to high-GGT cholestasis and DPM/CHF in vivo. In vitro, they can lead to centriolar and axonemal abnormalities. These observations indicate that mutation in *ZFYVE19* results, through as yet undefined mechanisms, in a ciliopathy.

## INTRODUCTION

Congenital hepatic fibrosis (CHF) comprises a set of developmental abnormalities that are part of many disease phenotypes.<sup>1</sup> Histopathological study in CHF finds fibrosis of portal tracts, usually without inflammation; hypoplasia of portal venules; and increased numbers of bile-duct profiles, usually with luminal dilatation, and often at portal-tract margins. This pattern is termed the ductal plate

malformation (DPM).<sup>2</sup> The major sequela of CHF is portal hypertension (PH), often clinically manifested as splenomegaly, hypersplenism and variceal bleeding. CHF reflects dysfunction of primary cilia<sup>3</sup> and often is accompanied by malformations in other organs or malfunctions in other systems. Most ciliopathies with DPM/CHF manifest cholestasis only when complicated by infection or obstruction of the biliary tract,<sup>4,5</sup> excepting double-cortin domain-containing protein 2 (*DCDC2*) disease,<sup>6</sup> tetratricopeptide repeat domain 26 disease<sup>7</sup> and perhaps polycystic kidney disease 1-like 1-related 'syndromic' biliary atresia.<sup>8</sup> Kinesin family member 12 (*KIF12*) disease and protein phosphatase 1F (*PPM1F*) disease are putative cholangiociliopathies. Histopathological features of portal tracts are not described in *PPM1F* disease and in *KIF12* disease do not suggest DPM/CHF.<sup>9,10</sup>

Forms of intrahepatic cholestasis can be categorised by whether levels of serum gamma-glutamyl transferase (GGT) activity rise together with serum concentrations of conjugated bilirubin or remain in normal ranges despite hyperbilirubinaemia. Higher GGT values often reflect inflammatory cholangiopathy, as with Alagille syndrome, ATP binding cassette subfamily B member 4 (*ABC4*) disease, extrahepatic biliary atresia, Langerhans cell histiocytosis and neonatal sclerosing cholangitis (*CLDN1*, *DCDC2*, *KIF12* or *PPM1F* disease).<sup>6,11–16</sup> While high-GGT intrahepatic cholestasis in many paediatric patients can be ascribed to defects in known genes, substantial numbers of such patients remain without genetic diagnoses.

We sought to identify genes mutated in children with idiopathic high-GGT intrahepatic cholestasis. Through whole-exome sequencing (WES) and targeted Sanger sequencing (TSS), we detected pathogenic biallelic mutations in *ZFYVE19* in a subset of these patients. This report describes our genetic, clinical and histopathological studies in this subset, as well as observations suggesting ciliopathy in cultured cells lacking *ZFYVE19*.

## METHODS

### Patients

From 2004 to 2017, this study enrolled 25 Han Chinese patients (P; [table 1](#)) at Children's Hospital and Jinshan Hospital of Fudan University

(Shanghai, China). All were children; all had undiagnosed intrahepatic cholestasis and high GGT values (>100 U/L, expected range 7–50 U/L). Patients with congenital viral infections, cystic renal disease or radiologically demonstrated sclerosing cholangitis were excluded. A final patient (P30, [table 1](#)) was referred to us after cohort assembly. Two cohorts of children were used as controls. ‘Other liver’ controls (n=45) had either normal-GGT intrahepatic cholestasis or liver disease without cholestasis. ‘Non-liver’ controls (n=299) had no hepatobiliary disease.

### Genetic analysis

Genomic DNA materials were extracted by QIAamp DNA Blood Mini Kit (51106, Qiagen, Hilden, Germany) from the peripheral blood of patients and available family members (parents and siblings, all healthy). WES was performed in 18 patients and the two control groups with the same sequencing platform (Genesky Biotechnologies, Shanghai, China);<sup>17</sup> WES for P30 was conducted elsewhere (WuXi NextCODE, Shanghai, China). Total WES depth was 100×. WES data were screened for candidate mutations with a routine filtering procedure (online supplementary figure S1).<sup>18</sup> Polyphen2, Sorting Intolerant from Tolerant (SIFT) and MutationTaster were used to predict the pathogenicity of candidate variants.<sup>19</sup> TSS was performed to confirm variants identified by WES, with primers for PCR amplification listed in online supplementary table S1. For patients with insufficient DNA materials, only TSS was performed to screen for mutations of candidate genes. Sequencing approaches for each patient are listed in online supplementary table S2.

### mRNA and protein sequence analysis

ZFYVE19 mRNA sequence (NM\_001077268) was analysed by online servers ORFfinder,<sup>20</sup> ATGpr<sup>21</sup> and ESTScan<sup>22</sup> to identify translation initiation sites, and using G4hunter,<sup>23</sup> G4IPDB<sup>24</sup> and QGRS Mapper<sup>25</sup> to identify G-quadruplexes. The ZFYVE19 protein sequences of *Homo sapiens* and eight orthologues (*Pan troglodytes*, *Canis lupus*, *Bos taurus*, *Mus musculus*, *Rattus norvegicus*, *Gallus gallus*, *Xenopus tropicalis* and *Dario rerio*) were retrieved from the National Centre for Biotechnology Information. Alignment of protein sequences was performed by Multiple Sequence Comparison by Log-Expectation (MUSCLE).<sup>26</sup> The sequence logo was created by Jalview<sup>27</sup> and WebLogo.<sup>28</sup>

### Histological and immunohistochemical studies

Native-liver biopsy specimens (n=7; P1, P4, P5, P7, P14, P25 and P28) and explanted-liver specimens (n=3; P14, P29 and P30) were reviewed for histopathological studies. Formalin-fixed and paraffin-processed tissue sections (4 µm) were routinely stained with H&E. Sections also were immunostained with antibodies against the cholangiocyte-associated antigens cytokeratin (CK) 7 (monoclonal mouse anti-human, OV-TL12/30, ready-to-use; Agilent, Santa Clara, California, USA) and CK19 (P14, P25 and P29) (monoclonal mouse anti-human, RCK108, ready-to-use; Agilent) and the ciliary antigens acetylated alpha-tubulin (ACALT) (mouse monoclonal antibody, T7451 clone 6-11B-1, 1:7500 dilution; Sigma-Aldrich, Taufkirchen, Germany) and DCDC2 (mouse monoclonal antibody, sc-166051, 1:100 dilution; Santa Cruz Biotechnology, Dallas, Texas, USA; P4, P5, P14, P25 and P29). Liver specimens without any known disease from two adults (surplus at liver donation) and from a child with cholestatic *ABCB4* disease were immunostained as controls.

### Expression constructs

The coding sequence of human full-length (FL) ZFYVE19 (isoform uc001zmt.1) fused with an N-terminal hexahistidine

(His) tag and a C-terminal DYKDDDDK (FLAG) tag was synthesised (General Biosystems, Chuzhou, China). The synthesised DNA was cloned into the pcDNA3.1 vector (Thermo Scientific, Rockford, Illinois, USA) to form the construct ZFYVE19-FL for the expression of a 60 kD ZFYVE19 with an N-terminal His and a C-terminal FLAG. The c.112\_113insGGGGC insertion and c.226A>G mutation were introduced into the ZFYVE19-FL construct using KOD-Plus-Mutagenesis Kit (SMK-101; Toyobo Biotech, Shanghai, China), according to the manufacturer's protocol, to form the constructs ZFYVE19-insGGGGC and ZFYVE19-M76V. All constructs were verified by Sanger sequencing.

### Transient transfection

HeLa cells were cultured in Dulbecco's modified Eagle's medium (DMEM; Corning, Corning, New York, USA) supplemented with 10% foetal bovine serum (FBS, Corning). After cells attained 50%–60% confluency, transient transfections were carried out using PolyJet In Vitro DNA Transfection Reagent (SignaGen Laboratories, Rockville, Maryland, USA) according to the manufacturer's protocol. The pcDNA3.1 empty vector was also transfected as a negative control. Cells were harvested 48 hours after transfection to allow protein overexpression.

### Short hairpin RNA constructs and stable ZFYVE19-knockdown cells

To knock down endogenous expression of ZFYVE19, three short hairpin RNAs (shRNAs) were designed and cloned into lentiviral vector pHLV-U6-MCS-CMV-ZsGreen-PGK-PURO (Hanbio, Shanghai, China) to produce lentivirus. A human telomerase reverse transcriptase-immortalised retinal pigmented epithelial cell line (hTERT-RPE1, ATCC CRL-4000; ATCC, Manassas, Virginia, USA; ‘hRPE1 cells’) was maintained in DMEM/F12 medium (1:1) with L-glutamine and 15 mM HEPES (Corning) supplemented with 10% FBS (Corning). Particles of shRNA lentivirus and of scrambled shRNA control lentivirus were added to the culture medium at a multiplicity of infection of 30 when cells were grown to 50% confluence. Puromycin, 50 µM (Selleck, Shanghai, China), was added to the culture medium 48 hours after infection. After 7 days of puromycin selection to enrich cultures in stably transfected cells, the cells were harvested to assess ZFYVE19 knockdown efficiency by western blot (online supplementary figure S2).

### Fibroblast-like cells derived from patient-induced pluripotent stem cells (iPSCs)

iPSCs were generated from peripheral blood mononuclear cells of P14 as described (Gemple Biotech, Shanghai, China).<sup>29</sup> A normal karyotype (46,XY) was confirmed by G-banding of metaphase chromosomes with an approximate resolution of 300–400 bands per haploid genome using standard procedures.<sup>29</sup> Expression of typical pluripotency markers NANOG, OCT4, SOX2 and TRA-1–60 was confirmed by immunofluorescence staining. The homozygous ZFYVE19 nonsense mutation c.314C>G was retained, as confirmed by Sanger sequencing. Fibroblast-like cells were derived as described.<sup>30</sup>

### Immunofluorescence microscopy analysis

For immunofluorescence microscopy analysis, cells were seeded onto glass coverslips in six-well plates and cultured in DMEM/F12 medium (1:1) with L-glutamine and 15 mM HEPES supplemented with 10% FBS. When cells attained 80%–90% confluence, they were cultured in serum-free media for another 2 days

**Table 1** Clinical and histopathological features, summarised, of studied children with high-GGT intrahepatic cholestasis

P/F	Sex/age at presentation	First symptoms	Evolution	Histopathological features	Response to UDCA 15–20 mg/kg/day	Outcome	Genetic diagnosis
P1/F1	♂/birth	J	Resolved J, 8 months; H, S, UGIH	Explanted liver, micronodular cirrhosis, ductular reaction (by report, not reviewed)	Uncertain; UDCA started at 4 years, 11 months but taken intermittently	LT at 5 years, 6 months	ZFYVE19 disease
P2/F2	♂/2 months	J	Resolved J, 4 months; pruritus, H, S	Micronodular cirrhosis	Intermediate; UDCA started at 6 years	Improved LFTs on UDCA at 9 years	Undiagnosed
P4/F4	♀/5 years	H, S	H, S, PH	DPM	Positive; UDCA started at 5 years	Improved LFTs on UDCA at 15 years, worsened on UDCA at 17 years	ZFYVE19 disease
P5/F4	♀/14 months	H	H	DPM	Positive; UDCA started at 14 months, stopped at 10 years, 5 months	Improved LFTs on UDCA at 10 years, 4 months; UDCA stopped at 12 years, 4 months	ZFYVE19 disease
P6/F5	♂/14 months	H, S, steatorrhea	H, S, PH	Extensive portal fibrosis with mixed inflammatory infiltration	Positive; UDCA started at 2 years	Normalised LFTs on UDCA at 3 years	Undiagnosed
P7/F6	♂/40 days	J, diarrhoea	Pruritus, H, PH	DPM	Intermediate; UDCA started at 3.5 years	Improved LFTs on UDCA at 14 years, 1 month	ZFYVE19 disease
P8/F7	♂/2.5 years	J, H, fever	H, S	Portal widening and fibrosis, ductular reaction	Positive; UDCA started at 3 years	Normalised LFTs on UDCA at 5 years	Undiagnosed
P9/F8	♂/2.5 years	J, H	Pruritus, H, S, liver failure	Micronodular cirrhosis, ductular reaction	Negative; UDCA started at 3 years	Death at 4 years	Undiagnosed
P10/F9	♂/birth	J	Normalised	ND	Positive; UDCA started at 2 months	Normalised LFTs at 8 years; UDCA stopped at 5 months	Undiagnosed
P14/F13	♂/4 months	Fever, diarrhoea	H, S, PH, UGIH	DPM, cholestasis	Positive; UDCA started at 1 year, 4 months	LT at 6 years, 4 months	ZFYVE19 disease
P15/F14	♀/2 days	J	J, H, S, PH,	ND	Positive; UDCA started at 22 days	Normalised LFTs on UDCA at 11 months	Undiagnosed
P16/F15	♂/12 years	H, S, thrombocytopenia	H, S, PH, thrombocytopenia	Portal widening and fibrosis, ductular reaction	Positive; UDCA started at 12 years, 5 months	Normalised LFTs on UDCA at 15 years	Undiagnosed
P17/F16	♀/1 year	Fever, cough, diarrhoea	Pruritus, H, S, PH	Extensive portal fibrosis with mixed inflammatory infiltration	Intermediate; UDCA started at 3 years, 5 months	Improved LFTs on UDCA at 4 years	Undiagnosed
P18/F16	♂/4 months	Fever, cough	H, S	Extensive portal fibrosis with mixed inflammatory infiltration, ductular reaction	Intermediate; UDCA started at 1y8mo	Improved LFTs on UDCA at 2y	Undiagnosed
P19/F17	♂/1 year, 9 months	Cough	H, S	Ultrastructural features of glycogen storage disease	Uncertain; UDCA started at 1 year, 10 months	LT at 5 years, 4 months	Undiagnosed
P20/F18	♀/1 month	J	J, H, S	Portal fibrosis with mixed inflammatory infiltration, ductular reaction, cholestasis	Positive; UDCA started at 1 month, 15 days	Normalised LFTs at 15 months; UDCA stopped at 9 months	Undiagnosed
P21/F19	♀/1 month	J	J, F, H, S	ND	Uncertain; UDCA started at 6 months but taken intermittently	LT at 8 months	Undiagnosed
P22/F20	♀/1 w	J	H, S	Chronic inflammation, intrahepatic bile-duct paucity	Uncertain; UDCA started at 1 year, 3 months	Unimproved LFTs on UDCA at 4 years, 4 months	Undiagnosed
P23/F21	♂/1 week	J	H, S	Portal inflammatory infiltration	Uncertain; UDCA started at 1 month	Lost to follow-up	Undiagnosed
P24/F22	♂/2 days	J	H, S	Spotty necrosis, with mixed inflammatory infiltration	Uncertain; UDCA started at 1 month, 20 days	Lost to follow-up	Undiagnosed
P25/F23	♂/3 months	J	H, S	Portal widening and fibrosis, ductular reaction	Positive; UDCA started at 4 years	Normalised LFTs on UDCA at 6 years	ZFYVE19 disease
P26/F24	♂/6 months	Fever	H, S	Portal widening and fibrosis, ductular reaction	Positive; UDCA started at 1 year	Improved LFTs on UDCA at 3 years, 8 months	Undiagnosed
P27/F25	♂/3 days	J	H	Portal widening and fibrosis, ductular reaction	Positive; UDCA started at 1 month	Improved LFTs on UDCA at 1 year, 7 months	Undiagnosed
P28/F26	♀/9 years	H, S	H, S	Biopsy, DPM	Positive; UDCA started at 10 years	Improved LFTs on UDCA at 11 years	ZFYVE19 disease
P29/F26	♀/4 years	UGIH	H, S	DPM, fibro-obliterative loss of bile ducts with DPM	No UDCA	LT at 4 years, 8 months	ZFYVE19 disease
P30/F27	♂/3 months	Fever, cough	H, S, PH, UGIH	DPM, fibro-obliterative loss of bile ducts with DPM, cholestasis	Positive; UDCA started at 3 months	LT at 1 year, 10 months	ZFYVE19 disease

UDCA response is defined as negative when no improvement was observed in LFTs, intermediate when partial improvement was observed in LFTs and positive when LFT values returned to normal. Histopathological findings are summarised from original reports or, when feasible, on review of sections.

♂, male; ♀, female; DPM, ductal plate malformation; F, family; GGT, gamma-glutamyl transferase; H, hepatomegaly; J, jaundice; LFT, liver function test; LT, liver transplantation; ND, not done; P, patient; PH, portal hypertension; S, splenomegaly; UDCA, ursodeoxycholic acid; UGIH, recurrent upper gastrointestinal haemorrhage.

(‘serum starvation’) to induce cell cycle G1-phase/G0-phase synchronisation, accompanied by ciliogenesis.<sup>31</sup> Cells were fixed and permeabilised with ice-cold methanol for 10 min, then immunostained with antibody against the ciliary component ADP-ribosylation factor-like GTPase 13B (ARL13B; rabbit polyclonal antibody, 17711-1-AP, 1:1000 dilution; Proteintech, Wuhan, China) and the centriole marker  $\gamma$ -tubulin (mouse monoclonal antibody, T6557, 1:1000 dilution; Sigma-Aldrich). Goat anti-rabbit Alexa Fluor 488 (A27034) and goat anti-mouse Alexa Fluor 594 (R37117; both 1:1000 dilution; Thermo Scientific) were used as secondary antibodies. We examined the appearances of primary cilia and of centrioles in hRPE cells (both scrambled control and ZFYVE19 knockdown) and in fibroblast-like cells from P14 and a normal control.

Fluorescence images were acquired using a confocal laser scanning microscope (Olympus FluoView FV1000, New York, USA). Percentages of ciliation and of centriolar abnormality in each cell group ( $n > 100$ ) were determined in three independent experiments, and significance was determined by paired t-testing.

### Western blotting

Whole-cell lysates ( $1 \times 10^6$  cells) or whole-tissue lysates (50 mg human liver) in radioprecipitation assay buffer (50 mM Tris, 150 mM NaCl, 1% Triton X-100, 1% sodium deoxycholate and 0.1% sodium dodecyl sulfate (SDS)) with freshly added protease inhibitor (88625, Thermo Scientific) were routinely processed onto polyvinylidene difluoride membranes following 12% SDS-polyacrylamide gel electrophoresis. The resulting blots were probed with primary antibodies at 4°C overnight and with secondary antibodies at room temperature for 1 hour.

The primary antibodies used were directed against ZFYVE19 (rabbit polyclonal antibody, 23163-1-AP, 1:3000 dilution; Proteintech), the octapeptide epitope tag FLAG (rabbit polyclonal antibody, F7425, 1:500 dilution; Sigma-Aldrich), the multiple-histidine epitope tag His (mouse monoclonal antibody, A00186, 1:2000 dilution; Genscript, Nanjing, China) and beta-actin (mouse monoclonal antibody, 60008-1-Ig, 1:5000 dilution; Proteintech). Liver tissues were obtained at transplantation from two patients with ZFYVE19 mutations (P14 and P29) and seven patients with liver disease of other aetiologies (ABCB4 deficiency, aldo-keto reductase family one member D1 deficiency, non-syndromic biliary atresia, ATPase phospholipid transporting 8B1 deficiency, glycogen storage disease type Ia, neuroblastoma amplified sequence deficiency and Alagille syndrome).

### Statistical analysis

Statistical analyses were performed using software package STATA V.10, and Fisher’s exact test was employed to compare the frequency of mutated alleles between our patient cohorts and both ‘other liver disease controls’ and ‘non-liver controls’. P values of  $< 0.05$  were considered statistically significant.

## RESULTS

### Biallelic mutations in ZFYVE19: association with high-GGT intrahepatic cholestasis

Nine patients carrying biallelic ZFYVE19 mutations in homozygote or compound heterozygote form (figure 1A,B and table 1) were identified in this study. Autosomal recessive inheritance was confirmed by segregation of mutated alleles within pedigrees. In eight patients, WES data excluded mutations in genes associated with high-GGT cholestasis or CHF either in published reports or in unpublished data assembled at our institute (online supplementary table S3). Although individual patients harboured

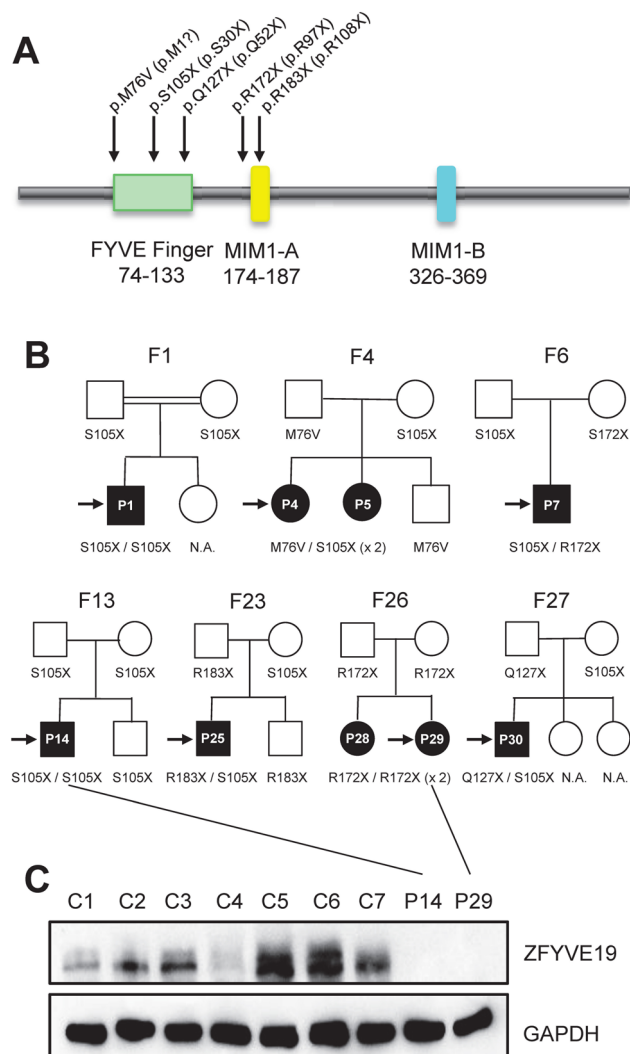


**Figure 1** ZFYVE19 protein, mutation sites; family pedigrees; and expression. (A) ZFYVE19 protein schema with mutation sites (AA). Renumbered mutation sites based on dAUG are indicated in parentheses. (B) Pedigrees, families with ZFYVE19 mutations. (C) Expression of ZFYVE19 in livers demonstrated by western blot. ZFYVE19 was absent from explanted livers of patients P14 and P29 and present in control livers (C1, ABCB4 deficiency; C2, AKR1D1 deficiency; C3, biliary atresia; C4, ATP8B1 deficiency; C5, glycogen storage disease type Ia; C6, NBAS deficiency; C7, Alagille syndrome). AA, amino acid; ABCB4, ATP binding cassette subfamily B member 4; dAUG, downstream AUG; N.A., unavailable sample. AKR1D1, aldo-keto reductase family one member D1; ATP8B1, ATPase phospholipid transporting 8B1; NBAS, neuroblastoma amplified sequence.

mutations in various other genes (online supplementary table S4), those genes have no established relationships with liver disease. Without sufficient material for WES in P1, only TSS was performed. This identified biallelic ZFYVE19 mutations. P1 had also been studied previously to exclude ABCB4 mutations.<sup>32</sup>

Five ZFYVE19 mutations were identified, including the two novel mutations c.226A>G and c.379C>T. The allele frequencies of the other three mutations, c.314C>G, c.514C>T and c.547C>T, were significantly higher in the patient cohorts than in control cohorts and in the Exome Aggregation Consortium (ExAC) and gnomAD databases (table 2). The incidence of biallelic ZFYVE19 mutations in the patient cohort is 26%, which is significantly higher than those in the ‘other liver controls’ (6/23 vs 0/45,  $p = 0.0026$ ) and the non-liver controls (6/23 vs

**Table 2** Mutations identified in *ZFYVE19* (NM\_001077268)

Nucleotide change	Genome position (GRCh37/hg19)	dbSNP rs#	Amino acid change	ExAC	gnomAD	Allele frequency			P value of allele frequency (Fisher's exact test)	
						Patient cohort	Other liver control	Non-liver control	Patient cohort versus other liver control	Patient cohort versus non-liver control
c.226A>G	chr15:41 100 013	N.A.	p.M76V	N.A.	N.A.	1/44	0/90	0/598	0.333	0.070
c.314C>G	chr15:41 101 351	rs769683740	p.S105X	10/1 20 716	1.4e-5	7/44	0/90	1/598	2.92e-04	3.37e-08
c.379C>T*	chr15:41 101 416	N.A.	p.Q127X	N.A.	N.A.	N.A.	N.A.	N.A.	N.A.	N.A.
c.514C>T	chr15:41 102 111	rs769683740	p.R172X	1/1 20 750	1.4e-5	3/44	0/90	0/598	0.034	3.02e-04
c.547C>T	chr15:41 102 144	rs771251472	p.R183X	1/1 20 744	6.98e-6	1/44	0/90	0/598	0.333	0.070

\*The mutation c.379C>T was identified only in P30, who was enrolled after initial patient cohort assembly. Allele frequency of c.379C>T was not calculated. ExAC, Exome Aggregation Consortium; N.A, not available.

0/299,  $p < 0.0001$ ). Our data thus demonstrate an association between biallelic *ZFYVE19* mutations and high-GGT intrahepatic cholestasis.

### Alternative translation–initiation site: identification, confirmation and implications

G-quadruplexes were identified at guanine-rich regions of *ZFYVE19* (figure 2A). Translation initiation by the annotated AUG was likely to be inhibited by the presence of G-quadruplexes, which are stable translation-inhibiting secondary structures mostly situated in 5' un-translated regions.<sup>33–35</sup> The 5-base polymorphism c.112\_113insGGGGC (rs142730574) was recorded in ExAC with high frequencies of 35.55% for heterozygotes and 12.6% for homozygotes. It had no functional consequence. This indicated a downstream AUG (dAUG) with optimal Kozak context as an alternative translation–initiation site for the translation of a 396-amino acid (AA) isoform of *ZFYVE19* (BC021092)<sup>36</sup> starting from methionine-76 (M76). The residue M76 was strongly conserved across species (figure 2B).

Translation initiation of *ZFYVE19* protein from M76 was confirmed by in vitro overexpression of constructs *ZFYVE19*-FL and *ZFYVE19*-insGGGGC, shown as a 50 kD band on western blotting (figure 2C,D). Translation initiation from M1 was only observed in vitro with forced overexpression and not in vivo (figure 1C and online supplementary figure S3), consistent with a fully functional 396-AA isoform translated from dAUG. In this functional isoform, the mutation c.226A>G, p.M76V would disrupt translation initiation (c.1A>G, p.M1?). By this reworked numbering scheme, the other four mutations were designated as c.314C>G, p.S105X/c.89C>G, p.S30X; c.379C>T, p.Q127X/c.156C>T, p.Q52X; c.514C>T, p.R172X/c.289C>T, p.R97X; c.547C>T, p.R183X/c.322C>T, p.R108X (figure 1A). All five mutations thus predictedly cause complete loss of function in *ZFYVE19*.

### Patients with *ZFYVE19* mutations: clinical and imaging study features

All nine children with biallelic *ZFYVE19* mutations were born at term, with normal weight, following an uneventful pregnancy. Only in F1 (P1) was parental consanguinity acknowledged. There were two pairs of siblings (P4 and P5, P28 and P29). None of the seven families knew of a genealogical link to any other.

Seven patients were referred to us for evaluation of abnormal hepatobiliary-disease biomarker values with PH and its sequelae, such as hepatosplenomegaly (n=6; P1, P4, P7, P14, P25 and P30) and/or upper gastrointestinal (GI) tract bleeding (n=4; P1, P14, P29 and P30). Two patients were identified on family

screening: In P5, the sibling of P4, biomarker values were noted to be abnormal, with hepatomegaly found on further evaluation; in P28, the sibling of P29, hepatosplenomegaly was noted, with abnormal biomarker values on further evaluation.

P4, P14 and P28 had thrombocytopenia ascribed to hypersplenism. No child was icteric at enrolment in the study, although P1, P7, P25 and P30 had been jaundiced as neonates. GGT was elevated in all nine, as were serum alanine transaminase (ALT) and aspartate transaminase (AST) activities (table 3). All patients had undergone ultrasonography and P4, P14 and P25 had undergone magnetic resonance cholangiopancreatography. None had signs of large bile-duct sclerosing cholangitis. No patient underwent endoscopic cholangiopancreatography. Neither nephromegaly nor frank renal cystic change was identified in any of the nine patients. Four patients (P1, P14, P29 and P30) underwent LT for recurrent GI bleeding. Hepatocellular synthetic function was generally preserved, even in those patients who underwent LT.

Seven patients (P1, P4, P5, P7, P14, P25 and P30) received ursodeoxycholic acid (UDCA), 15–20 mg/kg/day. ALT, AST and GGT values fell to expected ranges with UDCA treatment in all. In three patients who temporarily discontinued UDCA, ALT, AST and GGT values flared (P1, P4 and P5; table 3). Although P14 had continuously received UDCA for 5 years, with biomarkers in normal ranges, GI haemorrhage recurred and liver transplantation (LT) was required at age 6 years, 4 months (survival to date, without disease, 4 months). Biomarker values similarly normalised in P1 at age 4 years, 11 months, with initiation of UDCA therapy, but GI haemorrhage recurred after UDCA treatment was interrupted for 1 month. He underwent LT at age 5 years, 6 months (survival to date, without disease, 14 years). P29, managed elsewhere, never received UDCA. She underwent LT at age 4 years, 8 months (survival to date, without disease, 12 months). P30 had continuously received UDCA since age 3 months, with improvement in biochemical profile. However, GI haemorrhage recurred, and the patient underwent LT aged 22 months (survival to date, without disease, 2 months).

### Histopathological findings

The seven liver-biopsy specimens, all percutaneous, necessarily sampled peripheral liver. They included interlobular and small septal portal tracts with lobule. The portal tracts were expanded by fibrosis without oedema or substantial inflammation. They and the draining venules were irregularly disposed, rather than equidistantly spaced from one another. The portal tracts generally contained increased numbers of bile-duct profiles. These were not ectatic. However, portal-vein radicles were small or

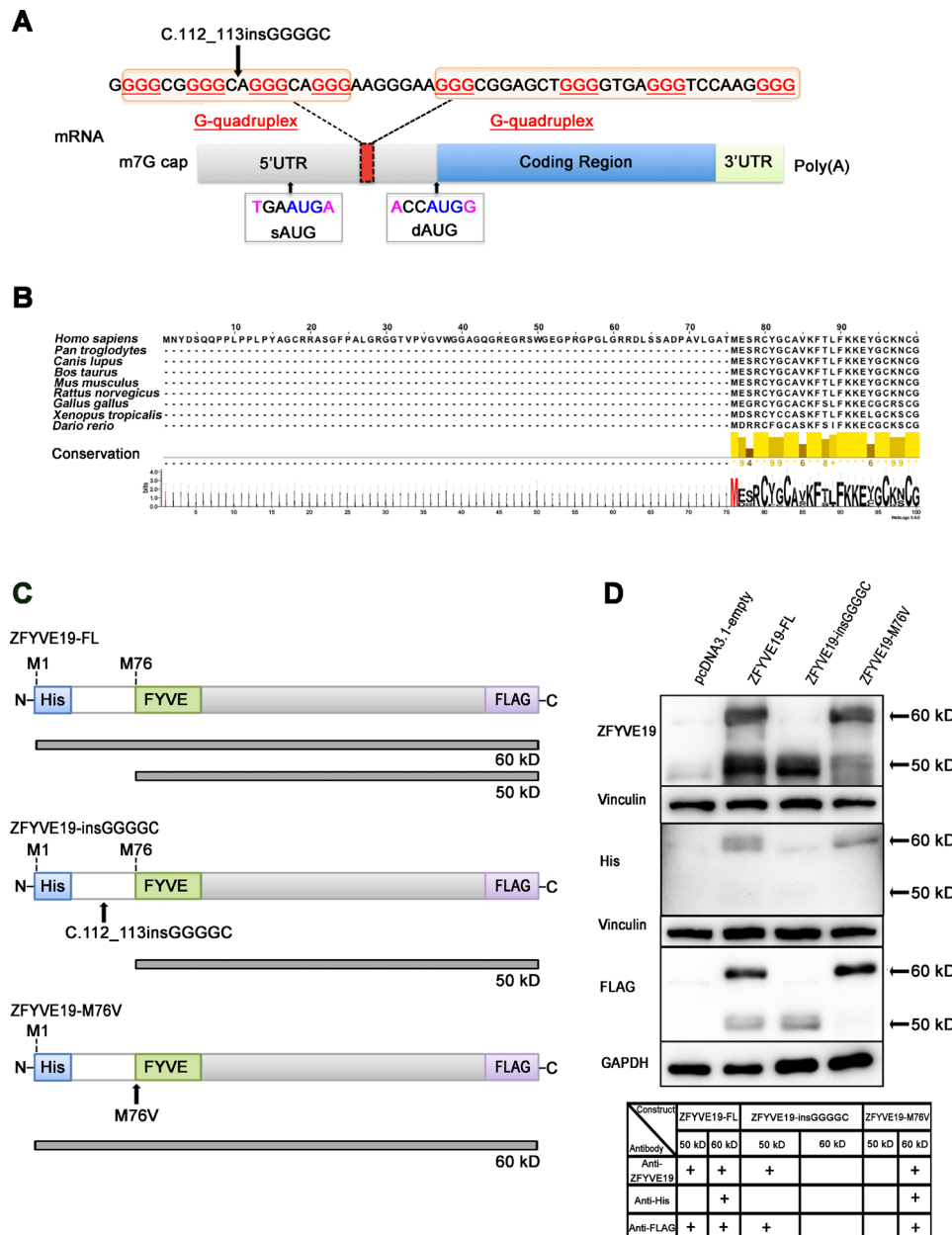


**Figure 2** *ZFYVE19*, its variants and its expression. (A) mRNA schema. The identified G-quadruplex, sAUG and dAUG are indicated. (B) The residue M76 is conserved across species. (C) Diagram of expression constructs ZFYVE19-FL, ZFYVE19-M76V and ZFYVE19-insGGGGC. The sites of the His tag, FLAG tag, mutation M76V and c.112\_113insGGGGC are shown, and the overexpressed proteins are also illustrated with their sizes in western blot profiles. (D) Western blot profiles of overexpressed ZFYVE19 isoforms detected by anti-ZFYVE19, anti-His and anti-FLAG antibodies. A 60 kD band was detectable in HeLa cells transfected with expression constructs ZFYVE19-FL and ZFYVE19-M76V (detected by antibodies against ZFYVE19, the His tag and the FLAG tag). The 60 kD band was not detected for construct ZFYVE19-insGGGGC, confirming that c.112\_113insGGGGC abolishes expression of the 471-AA-long ZFYVE19 isoform. A 50 kD band was demonstrable for constructs ZFYVE19-FL and ZFYVE19-insGGGGC using anti-ZFYVE19 and anti-FLAG antibodies, but was not detectable with anti-His antibody, as the N-terminal His tag was not expressed when translation was initiated from dAUG. dAUG, downstream AUG; sAUG, annotated AUG.

lacking. Lobular disarray and inflammation were not encountered. Sinusoids and draining venules were architecturally unremarkable. Although accumulations of bile pigment were not observed at any site, metallothionein deposits were found in juxtportal hepatocytes. These findings were consonant with the DPM and with chronic anicteric cholestasis.

Samples from three explanted livers (P14, P29 and P30) included large and small septal portal tracts as well as interlobular portal tracts. Many of these were markedly broadened (figure 3A,B). Both large (figure 3A) and small (figure 3C) portal

tracts were again of note for hypoplasia or absence of portal venules. Hypoplasia of portal-vein branches was not apparent in large septal portal tracts (figure 3D). Irregularity in disposition of portal tracts and draining venules was evident. Bile-duct profiles were abnormal, with staghorn configurations (arrow, figure 3D). In some portal tracts, periductal fibrosis was found, occasionally with disarray of cholangiocytes. Attenuation and atypism of cholangiocytes were found in some smaller ducts, with atrophy and extinction (replacement by scar; arrows, figure 3C). Portal tracts were cuffed by bile ductules without neutrophil-leucocyte

**Table 3** Clinical findings and evolution of biomarkers in patients with *ZFYVE19* disease

Patient	Age at sampling	Liver texture on palpation/width below ribs in right midclavicular line	Spleen texture on palpation/width below ribs in left midclavicular line	TB/DB (μmol/L)	ALT/AST (U/L)	GGT (U/L)	ALB (g/L)	TBA (μmol/L)	UDCA administration
P1	4 years, 10 months	Stiff/1 cm	Stiff/6 cm	17/8	183/129	236	32.7	N.A.	None
	4 years, 11 months	N.A.	N.A.	18/5	26/17	44	43.1	N.A.	15 mg/kg/day
	5 years, 1 month	Stiff/1.5 cm	Stiff/5 cm	15.4/8	223/189	307	N.A.	N.A.	None
	5 year, 6 months	N.A.	N.A.	N.A. / N.A.	34/40	127	19.2	N.A.	None, LT at 5 years, 7 months
	7 years, 3 months	Not palpable	Not palpable	6.7/3.1	35/32	34	24	N.A.	None, 1 year, 8 months after LT
P4	4 years, 1 month	N.A.	N.A.	9.6/3.5	205/181	276	N.A.	N.A.	None
	5 years	Stiff/1.5 cm	Stiff/4.5 cm	10.4/4.6	292/203	279	N.A.	N.A.	None
	6 years	Stiff/1 cm	Stiff/4 cm	5.3/3.5	56/48	52	42.7	50.6	15 mg/kg/day
	8 years, 7 months	Stiff/1 cm	Stiff/3 cm	5.2/2.5	38/40	38	44.4	7.9	15 mg/kg/day
	11 years, 7 months	Not palpable	Stiff/5 cm	5.6/4.9	41/35	96	44.1	16.9	6 mg/kg/day
	15 years, 4 months	Not palpable	Stiff/5 cm	18.8/11.2	39/58	55	38	199.1	10 mg/kg/day
P5	17 years, 2 months	Not palpable	Stiff/3 cm	54.8/14.2	174/157	157	35.5	20.5	7 mg/kg/day
	1 year, 1 month	Stiff/3 cm	Not palpable	2.1/1.6	351/189	366	44.7	28.6	None
	2 years, 5 months	N.A.	N.A.	4.7/1.7	12/20	11	N.A.	10.2	10 mg/kg/day
	6 years, 6 months	N.A.	N.A.	5.8/2.2	110/75	69	44.4	6.7	None
	6 years, 7 months	N.A.	N.A.	5.9/2.0	38/32	42	44.5	28.0	10 mg/kg/day
	8 years, 10 months	Not palpable	Not palpable	3.7/1.7	9/5	32	44.2	25.3	10 mg/kg/day
P7	12 years, 4 months	Not palpable	Not palpable	7.1/1.3	95/37	131	43	2.4	None
	1 month, 25 days	N.A.	N.A.	48.4/44	77/119	756	43.7	182.3	None
	3 years, 9 months	Stiff/2 cm	Not palpable	11.4/3.1	39/89	487	47.7	41.5	15 mg/kg/day
	6 years, 2 months	Stiff/0.5 cm	Not palpable	4.7/1.8	14/25	137	44.6	21.3	30 mg/kg/day
	11 years, 11 months	Not palpable	Not palpable	6.4/3.1	23/16	46	45.7	5.1	15 mg/kg/day
P14	14 years, 1 month	Not palpable	Not palpable	14.1/5.2	39/27.9	50.8	46.7	20.3	15 mg/kg/day
	4 months, 16 days	N.A.	N.A.	4/2.5	66/87	364	43	N.A.	None
	1 year, 4 months	Stiff/4 cm	Stiff / 4.5 cm	5.5/2.3	45/194	424	47.4	28.4	None
	3 years, 3 months	Stiff/3 cm	Stiff / 3 cm	6.6/2.2	18/30	45	43.8	36.4	15 mg/kg/day
	5 years, 11 months	Stiff/0.5 cm	Stiff / 4.5 cm	6.4/2.3	71/72	68	41.7	N.A.	15 mg/kg/day
	6 years, 8 months	Stiff/5 cm	Stiff / 9 cm	11.1/3.2	20/38	–	40	–	15 mg/kg/day LT at 6 years, 4 months
P25	7 years, 5 months	N.A.	N.A.	5.8/1.9	126/54	192	46.4	4.4	None, after LT
	3 months, 1 day	N.A.	N.A.	114.5/72.3	273/171	N.A.	N.A.	124	None
	4 years	Soft/2 cm	Soft / 2 cm	29.2/23.2	225/173	481	39	98.8	None
	4 years, 3 months	Stiff/0.5 cm	Not palpable	20.1/12.4	126/127	317	44	141.2	15 mg/kg/day
	4 years, 6 months	Not palpable	Not palpable	17.5/3.5	43/58	103	36.3	N.A.	25 mg/kg/day
5 years, 3 months	Not palpable	Not palpable	9.1/4.5	56.7/70.6	121	35.2	N.A.	25 mg/kg/day	

Continued

Table 3 Continued

Patient	Age at sampling	Liver texture on palpation/width below ribs in right midclavicular line	Spleen texture on palpation/width below ribs in left midclavicular line	TB/DB (μmol/L)	ALT/AST (U/L)	GGT (U/L)	ALB (g/L)	TBA (μmol/L)	UDCA administration
P28	9 years, 5 months	Not palpable	Stiff/1 cm	27.3/10.2	69/64	239	42	38.2	None
	11 years, 2 months	Not palpable	Stiff/2.5 cm	35.6/11.8	27.9/45.2	42	42.5	21.3	12.5 mg/kg/day
P29	4 years, 5 months	N.A.	N.A.	N.A. / N.A.	95.8/101	282	27	N.A.	None
	4 years, 7 months	Stiff/2 cm	Stiff/1.5 cm	13.2/4.7	63/70	342	35.7	17.1	None, LT at 4 years, 8 months
	5 years, 4 months	Not palpable	Not palpable	17.2/3.1	15/43	10	41.4	2.7	None, 8 months after LT
P30	3 months, 3 days	Not palpable	Not palpable	38.3/32.7	93/92	753	–	71.7	None
	4 months, 13 days	Stiff/4 cm	Soft/3 cm	15.5/6.6	78/95	542	40.8	38.4	15 mg/kg/day
	1 year, 4 months	Stiff/3 cm	Stiff/6 cm	12.8/6.3	25/69	231	33.7	113.5	15 mg/kg/day
	1 year, 10 months	Stiff/1.5 cm	Stiff/4.5 cm	11.4/6.5	29/70.7	157	43.6	17	15 mg/kg/day
	1 year, 11 months	Not palpable	Not palpable	11.2/4.5	38/60.1	74.4	33.4	41.8	None, 3 weeks after LT
Expected values				5.1–17.1/0–6	0–40/0–40	7–50	35–55	0–10	

ALB, albumin; ALT, alanine transaminase; AST, aspartate transaminase; DB, direct bilirubin; GGT, gamma-glutamyl transferase; LT, liver transplantation; N.A., not available; P, patient; TB, total bilirubin; TBA, total bile acids; UDCA, ursodeoxycholic acid.

infiltrates, on occasion suggesting persistence of the ductal plate. Accumulations of bile pigment were present in some portal tracts (arrow, [figure 3E](#)), and metallothionein deposits again were present, extending several tiers of hepatocytes or deeper from portal tracts into the lobule ([figure 3F](#)). These findings were consonant with the DPM and with chronic cholestasis in the setting of sclerosing cholangiopathy other than usual autoimmune or primary sclerosing cholangitis.

### Immunohistochemical and western blot findings

Immunostaining for CK7 and CK19 alike highlighted bile ducts and ductules. Focal heterotopic expression of CK7 by hepatocytes remote from portal tracts was noted in explanted livers. In control material, expression of both ACALT and DCDC2 was demonstrated immunohistochemically, with intraluminal threadlike or dot-like marking suggesting axonemal location and without cytoplasmic expression ([figure 4A](#)). Such marking was markedly deficient or absent in patient materials, in which heterotopic expression within cytoplasm of cholangiocytes was found for both antigens ([figure 4B,C](#)). Immunostaining for ZFYVE19 was attempted, using several commercially available monoclonal and polyclonal antibodies, and was unsuccessful. Consistent with preferred use of the dAUG alternative translation–initiation site, no protein band corresponding to 50 kD was demonstrated in two patients’ explanted tissues (P14 and P29) by western blotting ([figure 1C](#)).

### Depletion of ZFYVE19 yields phenotypes with ciliary and centriolar abnormalities

As our histopathological and immunohistochemical findings suggested a ciliopathy, we assessed cilia-related phenotypes on ZFYVE19 depletion in hRPE1 and fibroblast cells, which are commonly adopted cell models for cilia study.<sup>37 38</sup> In ZFYVE19-knockdown hRPE1 cells, a prominent phenotypical abnormality, was an increase in numbers of basal bodies/centrioles ([figure 5A,B](#)), which in interphase control cells

existed as paired and closely approximated structures. Separation/abnormal arrangement of the centriole pair(s) was also observed ([figure 5A](#)). However, cilium assembly was not affected ([figure 5C](#)), and extra cilia took shape at extra basal bodies/centrioles ([figure 5A](#)). Similar phenotypes involving abnormalities of ciliary and centriolar numbers but not of cilium assembly were demonstrated in ZFYVE19-deficient fibroblast-like cells derived from patient iPSCs ([figure 5D–F](#)). Our data thus indicate that ZFYVE19 participates in cilia-related processes.

### DISCUSSION

Identification of a dAUG permitted us to demonstrate the preferential translation of a functional ZFYVE19 isoform initiated from M76. All five mutations found in ZFYVE19 patients lie in either the FYVE-type zinc finger domain or the MIM1-A motif that mediates the interaction between ZFYVE19 and vacuolar protein sorting-associated protein 4 (VPS4). They are predictedly pathogenic and likely cause complete loss of expression in ZFYVE19, either by disrupting translation initiation or via nonsense-mediated decay. Indeed, in patients with homozygous nonsense mutations (P14 and P29), we detected no ZFYVE19 expression in liver ([figure 1C](#)).

ZFYVE19 has been reported as a key regulator of abscission in cytokinesis, localised at the cleavage furrow and cytoplasmic-bridge midbody ring.<sup>39</sup> The midbody and centriole migrate after abscission to the same cell-surface site and participate in ciliogenesis. Interference with expression of ZFYVE19 causes abnormal chromosomal segregation and DNA damage. During interphase, ZFYVE19 locates mainly on centrosomes. G0 is a special phase of interphase, when the primary cilium emerges from the older centriole of a centrosome. As essential organelles, numbers of centrioles and primary cilia (two centrioles and one primary cilium per cell) are tightly controlled to subserve normal cell polarity, motility and signalling.<sup>40</sup> Our work in both hRPE1 cells and fibroblast-like cells (a cultured-cholangiocyte model was unavailable) demonstrated supernumerary centrioles

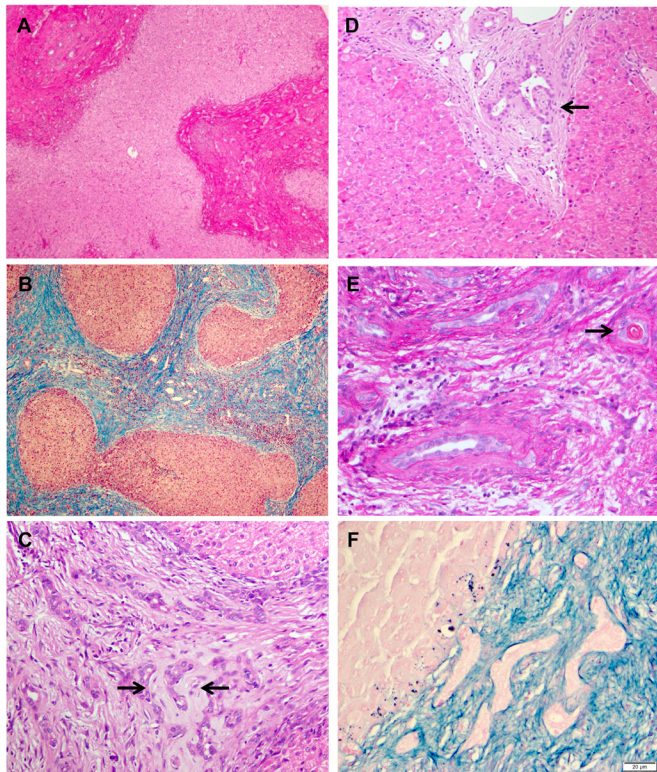


**Figure 3** Histopathological findings. CHF and DPM; bland parenchyma, markedly broadened portal tracts deficient in portal-vein radicles (A,B) and exhibiting dense fibrosis (B), bile-duct profiles in excess (C), with periductal hyalinisation (C, between arrows) and angulated ('staghorn') lumina (D, arrow); bile plugs in occasional ducts (E, arrow, again with periductal hyalinisation) and metallothionein deposits within juxtaseptal hepatocytes (F). Note in all the absence of 'interface activity': features of a hepatitis are lacking throughout. (A) Periodic acid–Schiff technique, original magnification  $\times 40$ ; (B) chromotrope aniline blue, original magnification  $\times 40$ ; (C,D) H&E, original magnifications  $\times 200$  and  $\times 100$ , respectively; (E) diastase–PAS technique, original magnification  $\times 200$ ; (F) Victoria blue, original magnification  $\times 100$ ; (A–F) representative images, P14 and P30. DPM, ductal plate malformation; CHF, congenital hepatic fibrosis.

and cilia when ZFYVE19 was depleted. We infer that in vivo as well ZFYVE19 deficiency leads to disruption of cilia-related processes or cilia-regulated pathways.<sup>41</sup>

Developmental and degenerative disorders caused by ciliary dysfunction, referred to as ciliopathies, affect various organs and systems and manifest diverse clinical features.<sup>42–43</sup> In liver, hepatocytes do not express cilia but cholangiocytes do. Their primary cilia extend into the bile-duct lumen. Changes in bile flow and composition are thought to be sensed through the primary cilium and translated into changes in the functions of cholangiocytes.<sup>44</sup> Mutations in genes encoding cilium-associated proteins may lead to hypoplasia of portal-vein radicles, increased fibrosis of portal tracts and proliferation of cholangiocytes (with bile ducts more numerous, larger in diameter and more peripherally sited within the portal tract than normal), a set of associated malformations loosely referred to, depending on appearance, as the DPM or as CHF.<sup>1</sup> Our patients with ZFYVE19 mutations on histopathological study had portal-tract abnormalities consonant with the DPM or CHF, with the companion of sclerosing cholangiopathy. We consider their disorder a novel ciliopathy and ascribe it to mutations in ZFYVE19.

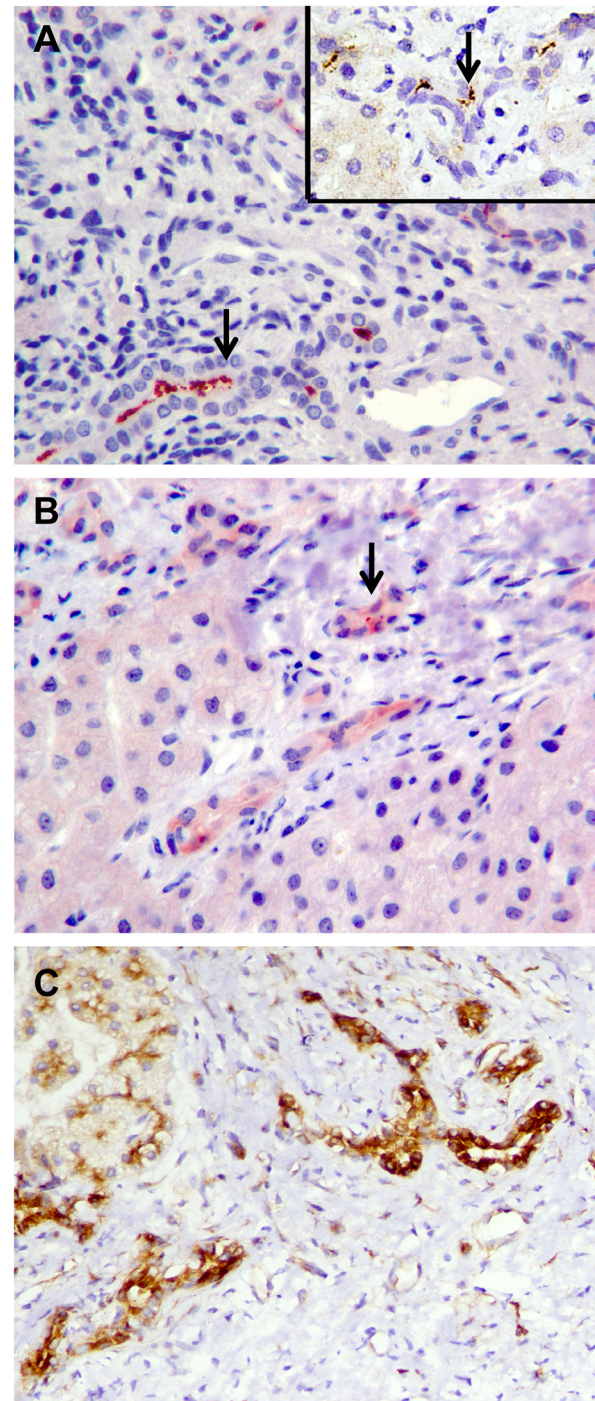


**Figure 4** Immunohistopathological findings. (A) In a control patient with ABCB4 deficiency, intraluminal bile-duct marking (arrows) is evident on immunostaining for DCDC2 (main image) and ACALT (inset image), which are constituents of the ciliary axoneme. Cholangiocyte cytoplasm does not mark. (B) Abnormal marking for DCDC2 in a patient with ZFYVE19 deficiency. Axonemal marking (arrow) is diminished, and cholangiocyte cytoplasm marks palely. (C) Abnormal marking for ACALT in a patient with ZFYVE19 deficiency. Axonemal marking is lacking, and cholangiocyte cytoplasm marks darkly. Additional pericanalicular ectopic expression of ACALT is visible in hepatocytes. All images, 3-amino-9-ethylcarbazole chromogen with haematoxylin counterstain; (A,B) original magnification  $\times 200$ ; (C) original magnification  $\times 100$ . ABCB4, ATP binding cassette subfamily B member 4; ACALT, acetylated alpha-tubulin; DCDC2, double-cortin domain-containing protein 2.

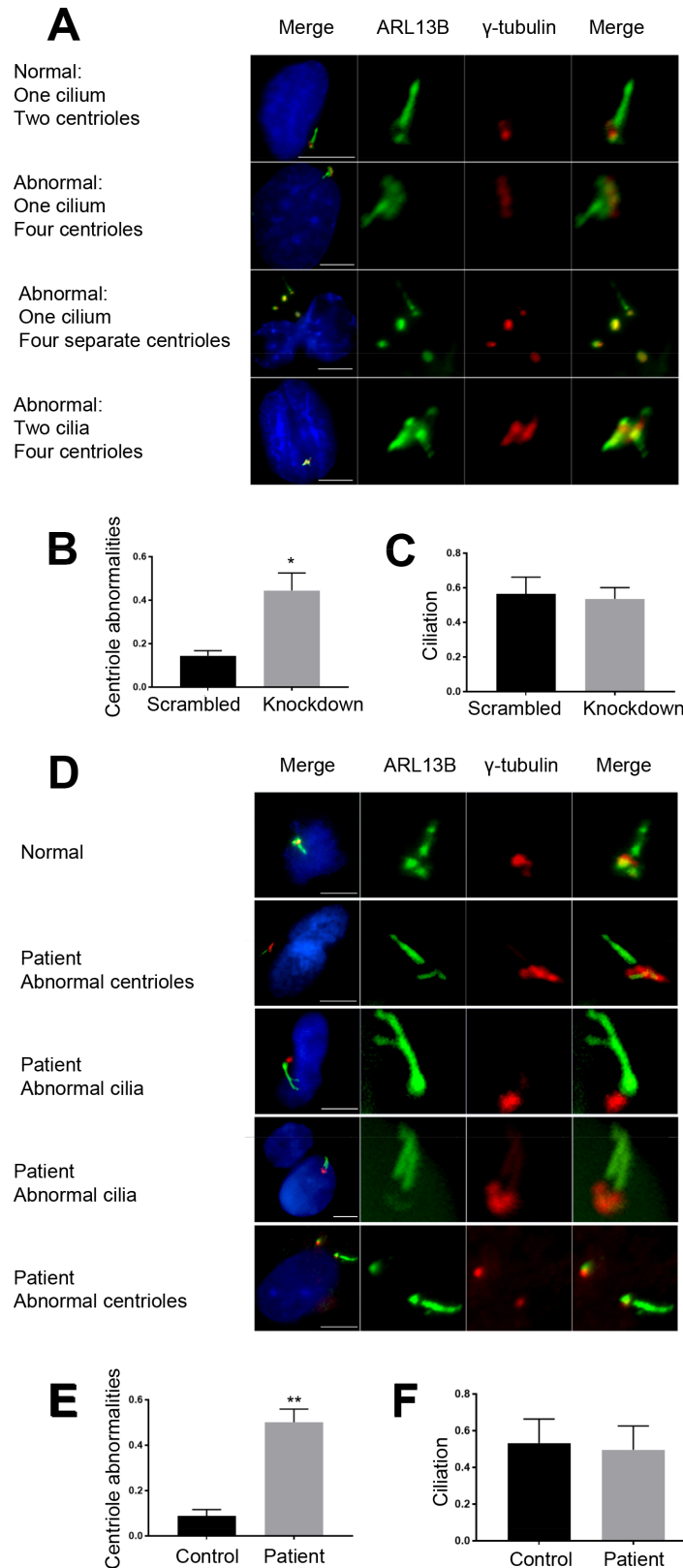


**Figure 5** Cilia-related phenotypes caused by depletion of ZFYVE19. (A) Representative images of ZFYVE19-knockdown hRPE1 cells. (B) Percentage of hRPE1 cells with abnormal basal bodies/centrioles, in comparison with the scrambled control. Significance was determined using paired t-testing. (C) Percentage of ciliated hRPE1 cells. (D) Representative images of ZFYVE19-deficient fibroblast-like cells derived from patient iPSCs. (E) Percentage of fibroblast-like cells with abnormal basal bodies/centrioles, in comparison with the normal control. Significance was determined using paired t-testing. (F) Percentage of ciliated fibroblast-like cells. (A,D) Centrioles and cilia were immunostained for ARL 13b (Alexa fluor 488, green) and  $\gamma$ -tubulin (Alexa fluor 594, red), respectively. DNA was stained with 4',6-diamidino-2-phenylindole (blue). Scale bar, 10  $\mu$ m. Two 'merge' panels demonstrate abnormal ciliary and centriolar numbers in a single cell—the first merge panel shows centrioles, cilia and nucleus; the second merge panel shows a closer view of centrioles and cilia. \* $P < 0.05$ , \*\* $P < 0.001$ . iPSC, induced pluripotent stem cell.

Their disorder is, however, unusual for ciliopathy in one clinical aspect. Ciliopathy that manifests with the DPM or CHF is not generally associated with elevated GGT values or with cholestasis (barring biliary-tract obstruction or infection), yet our patients were selected for high-GGT cholestasis. In addition, our patients had histopathological features of sclerosing cholangiopathy with cholestasis, including evidence of impaired biliary excretion of copper (inferred from deposits of copper-chelating metallothioneins). These changes suggest biliary-tract injury as an important manifestation of *ZFYVE19* disease. One other well-described ciliopathy, *DCDC2* disease, is similarly characterised by elevated GGT values and sclerosing cholangiopathy, although cholangiopathy in *DCDC2* disease includes large-duct lesions of a type not appreciated in our *ZFYVE19* disease patients. *DCDC2* is not known to localise at the ciliary base; immunostaining demonstrates it instead within the axoneme, where it is thought to interact with tubulin. The mechanisms by which *DCDC2* deficiency and *ZFYVE19* deficiency increase cholangiocyte susceptibility to injury are unclear.

Of interest is abnormal localisation of ciliary proteins *DCDC2* and *ACALT* in our patients' cholangiocytes. This might non-specifically reflect cholangiocyte injury (unpublished observations). Also possible, however, is that *ZFYVE19* acts in concert with *VPS4* at the intracytoplasmic functional barrier to free exchange of proteins between the cilium proper and the remainder of the cell.<sup>45 46</sup> Disruption of the coordinated function of *VPS4* and *ZFYVE19* might lead to diffusion of ciliary proteins into the wider cytoplasm.

Also of interest is the lack of clinically manifest extrahepatic disease in our patients, who of course were selected for a hepatobiliary phenotype. Full descriptions and analyses of extrahepatic disease in *DCDC2* disease patients with hepatobiliary disease as a predominating feature have yet to be published. However, mutation in *DCDC2* has been associated not only with neonatal sclerosing cholangitis<sup>13 14 47</sup> but also with intellectual deficiency,<sup>48 49</sup> hearing loss<sup>48</sup> and nephronophthisis.<sup>50</sup> Ciliopathies are, as a rule, multiorgan and multisystem disorders. We expect that as other patients with *ZFYVE19* mutations are studied, the disease phenotype will be extended to organs and systems outside the liver and biliary tract. In addition, we mean to monitor our patients with *ZFYVE19* disease to see if, as they grow, new effects of *ZFYVE19* deficiency appear. Given that abnormal chromosomal segregation and DNA damage follow *ZFYVE19* depletion *in vitro*,<sup>39</sup> we shall bear a hypothetically increased risk of malignancy in mind.

#### Author affiliations

<sup>1</sup>Department of Pediatrics, Jinshan Hospital of Fudan University, Shanghai, China

<sup>2</sup>The Center for Pediatric Liver Diseases, Children's Hospital of Fudan University, Shanghai, China

<sup>3</sup>Laboratory for Reproductive Health, Institute of Biomedicine and Biotechnology, Shenzhen Institutes of Advanced Technology, Chinese Academy of Sciences, Shenzhen, Guangdong, China

<sup>4</sup>Department of Surgery, Huashan Hospital Affiliated to Fudan University, Shanghai, China

<sup>5</sup>Department of Liver Surgery and Liver Transplantation Center, Ren Ji Hospital, School of Medicine, Shanghai Jiao Tong University, Shanghai, China

<sup>6</sup>Institutes of Biomedical Sciences, Fudan University, Shanghai, China

<sup>7</sup>Institut für Pathologie, Medizinische Universität Graz, Graz, Austria

**Contributors** Acquisition of data with analysis and interpretation of data involved W-SL (immunohistochemical and immunofluorescence studies), J-QL (genetic analysis), C-ZH (western blotting) and QW (immunofluorescence studies). W-SL and C-ZH were involved in the drafting of the manuscript; J-QL and C-ZH were involved in statistical analysis; J-YG, YQ, YL, C-HS, QX, XX, M-HZ and KA were involved in patient collection; QX was involved in study concept and design; ASK was involved in

histopathological analysis, immunohistochemical studies and critical revision of the manuscript; and J-SW was involved in obtaining funding, study concept and design, and study supervision.

**Funding** Support for this study was provided by the National Natural Science Foundation of China (grant numbers 81570468 and 81873543, to JW).

**Competing interests** None declared.

**Patient consent for publication** Not required.

**Ethics approval** The study was approved by the ethics committees of both hospitals and was in accordance with the ethical guidelines of the 1975 Declaration of Helsinki.

**Provenance and peer review** Not commissioned; externally peer reviewed.

**Data availability statement** Data are available upon reasonable request from J-SW (jshwang@shmu.edu.cn).

#### ORCID iDs

Weisha Luan <http://orcid.org/0000-0002-2130-6426>

Yi-Ling Qiu <http://orcid.org/0000-0002-7296-9115>

Kuerbanjiang Abuduxikuer <http://orcid.org/0000-0003-0298-3269>

#### REFERENCES

- Desmet VJ. What is congenital hepatic fibrosis? *Histopathology* 1992;20:465–78.
- Raynaud P, Tate J, Callens C, Cordi S, Vandersmissen P, Carpentier R, Sempoux C, Devuyt O, Pierreux CE, Courtoy P, Dahan K, Delbecq K, Lepreux S, Pontoglio M, Guay-Woodford LM, Lemaigre FP. A classification of ductal plate malformations based on distinct pathogenic mechanisms of biliary dysmorphogenesis. *Hepatology* 2011;53:1959–66.
- Gunay-Aygun M. Liver and kidney disease in ciliopathies. *Am J Med Genet C Semin Med Genet* 2009;151C:296–306.
- Shorbagi A, Bayraktar Y. Experience of a single center with congenital hepatic fibrosis: a review of the literature. *World J Gastroenterol* 2010;16:683–90.
- Gunay-Aygun M, Font-Montgomery E, Lukose L, Tuchman Gerstein M, Piwnicka-Worms K, Choyke P, Daryanani KT, Turkbey B, Fischer R, Bernardini I, Sincan M, Zhao X, Sandler NG, Roque A, Douek DC, Graf J, Huizing M, Bryant JC, Mohan P, Gahl WA, Heller T. Characteristics of congenital hepatic fibrosis in a large cohort of patients with autosomal recessive polycystic kidney disease. *Gastroenterology* 2013;144:112–21.
- Grammatikopoulos T, Sambrotta M, Strautnieks S, Foskett P, Knisely AS, Wagner B, Deheragoda M, Starling C, Mieli-Vergani G, Smith J, Bull L, Thompson RJ. University of Washington Center for Mendelian Genomics. Mutations in *DCDC2* (doublecortin domain containing protein 2) in neonatal sclerosing cholangitis. *J Hepatol* 2016;65:1179–87.
- Shaheen R, Alsahli S, Ewida N, Alzahrani F, Shamseldin HE, Patel N, Al Qahtani A, Alhebbi H, Alhashem A, Al-Sheddi T, Alomar R, Alobeid E, Abouelhoda M, Monies D, Al-Hussaini A, Alzouman MA, Shagrani M, Faqeih E, Alkuraya FS. Biallelic mutations in tetrapeptide repeat domain 26 (intraflagellar transport 56) cause severe biliary ciliopathy in humans. *Hepatology* 2020;71:2067–79.
- Berauer J-P, Mezina AI, Okou DT, Sabo A, Muzny DM, Gibbs RA, Hegde MR, Chopra P, Cutler DJ, Perlmutter DH, Bull LN, Thompson RJ, Loomes KM, Spinner NB, Rajagopalan R, Guthery SL, Moore B, Yandell M, Harpavat S, Magee JC, Kamath BM, Molleston JP, Bezerra JA, Murray KF, Alonso EM, Rosenthal P, Squires RH, Wang KS, Finegold MJ, Russo P, Sherker AH, Sokol RJ, Karpen SJ. Childhood Liver Disease Research Network (ChILDReN). Identification of polycystic kidney disease 1 like 1 gene variants in children with biliary atresia splenic malformation syndrome. *Hepatology* 2019;70:899–910.
- Maddirevula S, Alhebbi H, Alqahtani A, Algoufi T, Alsaif HS, Ibrahim N, Abdulwahab F, Barr M, Alzaidan H, Almehaideb A, AlSasi O, Alhashem A, Hussaini HA, Wali S, Alkuraya FS. Identification of novel loci for pediatric cholestatic liver disease defined by *KIF12*, *PPM1F*, *USP53*, *LSR*, and *WDR830S* pathogenic variants. *Genet Med* 2019;21:1164–72.
- Ünlüsoy Aksu A, Das SK, Nelson-Williams C, Jain D, Özbay Hoşnut F, Evirgen Şahin G, Lifton RP, Vilarinho S. Recessive Mutations in *KIF12* Cause High Gamma-Glutamyltransferase Cholestasis. *Hepatal Commun* 2019;3:471–7.
- Emerick KM, Rand EB, Goldmuntz E, Krantz ID, Spinner NB, Piccoli DA. Features of Alagille syndrome in 92 patients: frequency and relation to prognosis. *Hepatology* 1999;29:822–9.
- Oda T, Elkahoun AG, Pike BL, Okajima K, Krantz ID, Genin A, Piccoli DA, Meltzer PS, Spinner NB, Collins FS, Chandrasekharappa SC. Mutations in the human *Jagged1* gene are responsible for Alagille syndrome. *Nat Genet* 1997;16:235–42.
- Yi X, Han T, Zai H, Long X, Wang X, Li W. Liver involvement of Langerhans' cell histiocytosis in children. *Int J Clin Exp Med* 2015;8:7098–106.
- de Vree JM, Jacquemin E, Sturm E, Cresteil D, Bosma PJ, Aten J, Deleuze JF, Desrochers M, Burdelski M, Bernard O, Oude Elferink RP, Hadchouel M. Mutations in the *MDR3* gene cause progressive familial intrahepatic cholestasis. *Proc Natl Acad Sci U S A* 1998;95:282–7.

- 15 Hadj-Rabia S, Baala L, Vabres P, Hamel-Teillac D, Jacquemin E, Fabre M, Lyonnet S, De Prost Y, Munnich A, Hadchouel M, Smahi A. Claudin-1 gene mutations in neonatal sclerosing cholangitis associated with ichthyosis: a tight junction disease. *Gastroenterology* 2004;127:1386–90.
- 16 Delaunay J-L, Durand-Schneider A-M, Dossier C, Falguières T, Gautherot J, Davit-Spraul A, Aït-Slimane T, Housset C, Jacquemin E, Maurice M. A functional classification of Abcb4 variations causing progressive familial intrahepatic cholestasis type 3. *Hepatology* 2016;63:1620–31.
- 17 Wang N-L, Lu Y-L, Zhang P, Zhang M-H, Gong J-Y, Lu Y, Xie X-B, Qiu Y-L, Yan Y-Y, Wu B-B, Wang J-S. A specially designed multi-gene panel facilitates genetic diagnosis in children with intrahepatic cholestasis: simultaneous test of known large insertions/deletions. *PLoS One* 2016;11:e0164058.
- 18 Qiu Y-L, Gong J-Y, Feng J-Y, Wang R-X, Han J, Liu T, Lu Y, Li L-T, Zhang M-H, Sheps JA, Wang N-L, Yan Y-Y, Li J-Q, Chen L, Borchers CH, Sipos B, Knisely AS, Ling Y, Xing Q-H, Wang J-S. Defects in myosin Vb are associated with a spectrum of previously undiagnosed low  $\gamma$ -glutamyltransferase cholestasis. *Hepatology* 2017;65:1655–69.
- 19 Schwarz JM, Cooper DN, Schuelke M, Seelow D. MutationTaster2: mutation prediction for the deep-sequencing age. *Nat Methods* 2014;11:361–2.
- 20 Rombel IT, Sykes KF, Rayner S, Johnston SA. ORF-FINDER: a vector for high-throughput gene identification. *Gene* 2002;282:33–41.
- 21 Salamov AA, Nishikawa T, Swindells MB. Assessing protein coding region integrity in cDNA sequencing projects. *Bioinformatics* 1998;14:384–90.
- 22 Iseli C, Jongeneel CV, Bucher P. ESTScan: a program for detecting, evaluating, and reconstructing potential coding regions in EST sequences. *Proc Int Conf Intell Syst Mol Biol* 1999:138–48.
- 23 Bedrat A, Lacroix L, Mergny J-L. Re-evaluation of G-quadruplex propensity with G4Hunter. *Nucleic Acids Res* 2016;44:1746–59.
- 24 Mishra SK, Tawani A, Mishra A, Kumar A. G4IPDB: a database for G-quadruplex structure forming nucleic acid interacting proteins. *Sci Rep* 2016;6:38144.
- 25 Kikin O, D'Antonio L, Bagga PS. QGRS Mapper: a web-based server for predicting G-quadruplexes in nucleotide sequences. *Nucleic Acids Res* 2006;34:W676–82.
- 26 Edgar RC. Muscle: multiple sequence alignment with high accuracy and high throughput. *Nucleic Acids Res* 2004;32:1792–7.
- 27 Waterhouse AM, Procter JB, Martin DMA, Clamp M, Barton GJ. Jalview Version 2—a multiple sequence alignment editor and analysis workbench. *Bioinformatics* 2009;25:1189–91.
- 28 Crooks GE, Hon G, Chandonia J-M, Brenner SE. Weblogo: a sequence logo generator. *Genome Res* 2004;14:1188–90.
- 29 Meng X, Neises A, Su R-J, Payne KJ, Ritter L, Gridley DS, Wang J, Sheng M, Lau K-HW, Baylink DJ, Zhang X-B. Efficient reprogramming of human cord blood CD34+ cells into induced pluripotent stem cells with Oct4 and Sox2 alone. *Mol Ther* 2012;20:408–16.
- 30 Du S-H, Tay JC-K, Chen C, Tay F-C, Tan W-K, Li Z-D, Wang S. Human iPSC cell-derived fibroblast-like cells as feeder layers for iPSC cell derivation and expansion. *J Biosci Bioeng* 2015;120:210–7.
- 31 Chen M, Huang J, Yang X, Liu B, Zhang W, Huang L, Deng F, Ma J, Bai Y, Lu R, Huang B, Gao Q, Zhuo Y, Ge J. Serum starvation induced cell cycle synchronization facilitates human somatic cells reprogramming. *PLoS One* 2012;7:e28203.
- 32 Fang L-J, Wang X-H, Knisely AS, Yu H, Lu Y, Liu L-Y, Wang J-S. Chinese children with chronic intrahepatic cholestasis and high  $\gamma$ -glutamyl transpeptidase: clinical features and association with Abcb4 mutations. *J Pediatr Gastroenterol Nutr* 2012;55:150–6.
- 33 Bugaut A, Balasubramanian S. 5'-UTR RNA G-quadruplexes: translation regulation and targeting. *Nucleic Acids Res* 2012;40:4727–41.
- 34 Beaudoin J-D, Perreault J-P. 5'-UTR G-quadruplex structures acting as translational repressors. *Nucleic Acids Res* 2010;38:7022–36.
- 35 Gomez D, Guédin A, Mergny J-L, Salles B, Riou J-F, Teulade-Fichou M-P, Calsou P. A G-quadruplex structure within the 5'-UTR of TRF2 mRNA represses translation in human cells. *Nucleic Acids Res* 2010;38:7187–98.
- 36 Strausberg RL, Feingold EA, Grouse LH, Derge JG, Klausner RD, Collins FS, Wagner L, Shenmen CM, Schuler GD, Altschul SF, Zeeberg B, Buetow KH, Schaefer CF, Bhat NK, Hopkins RF, Jordan H, Moore T, Max SI, Wang J, Hsieh F, Diatchenko L, Marusina K, Farmer AA, Rubin GM, Hong L, Stapleton M, Soares MB, Bonaldo MF, Casavant TL, Scheetz TE, Brownstein MJ, Usdin TB, Toshiyuki S, Carninci P, Prange C, Raha SS, Loquellano NA, Peters GJ, Abramson RD, Mullahy SJ, Bosak SA, McEwan PJ, McKernan KJ, Malek JA, Gunaratne PH, Richards S, Worley KC, Hale S, Garcia AM, Gay LJ, Hulyk SW, Villalón DK, Muzny DM, Sodergren EJ, Lu X, Gibbs RA, Fahey J, Helton E, Kettman M, Madan A, Rodrigues S, Sanchez A, Whiting M, Madan A, Young AC, Shevchenko Y, Bouffard GG, Blakesley RW, Touchman JW, Green ED, Dickson MC, Rodriguez AC, Grimwood J, Schmutz J, Myers RM, Butterfield YSN, Krzywinski MI, Skalska U, Smailus DE, Schnerch A, Schein JE, Jones SJM, Marra MA, Mammalian Gene Collection Program Team. Generation and initial analysis of more than 15,000 full-length human and mouse cDNA sequences. *Proc Natl Acad Sci U S A* 2002;99:16899–903.
- 37 Oud MM, Bonnard C, Mans DA, Altunoglu U, Tohari S, Ng AYJ, Eskin A, Lee H, Rupar CA, de Wagenaar NP, Wu KM, Lahiry P, Pazour GJ, Nelson SF, Hegele RA, Roepman R, Kayserili H, Venkatesh B, Siu VM, Reversade B, Arts HH. A novel ICK mutation causes ciliary disruption and lethal endocrine-cerebro-osteodysplasia syndrome. *Cilia* 2016;5:8.
- 38 May-Simera HL, Wan Q, Jha BS, Hartford J, Kristov V, Dejene R, Chang J, Patnaik S, Lu Q, Banerjee P, Silver J, Insinna-Kettenhofen C, Patel D, Lotfi M, Malicdan M, Hotaling N, Maminshkis A, Sridharan R, Brooks B, Miyagishima K, Gunay-Aygun M, Pal R, Westlake C, Miller S, Sharma R, Bharti K. Primary cilium-mediated retinal pigment epithelium maturation is disrupted in ciliopathy patient cells. *Cell Rep* 2018;22:189–205.
- 39 Thoresen SB, Campsteijn C, Vietri M, Schink KO, Liestøl K, Andersen JS, Raiborg C, Stenmark H. ANCHR mediates Aurora-B-dependent abscission checkpoint control through retention of Vps4. *Nat Cell Biol* 2014;16:547–57.
- 40 Nigg EA, Holland AJ. Once and only once: mechanisms of centriole duplication and their deregulation in disease. *Nat Rev Mol Cell Biol* 2018;19:297–312.
- 41 Mahjoub MR, Stearns T. Supernumerary centrosomes nucleate extra cilia and compromise primary cilium signaling. *Curr Biol* 2012;22:1628–34.
- 42 Waters AM, Beales PL. Ciliopathies: an expanding disease spectrum. *Pediatr Nephrol* 2011;26:1039–56.
- 43 Oud MM, Lamers IJC, Arts HH. Ciliopathies: genetics in pediatric medicine. *J Pediatr Genet* 2017;6:018–29.
- 44 Masyuk AI, Masyuk TV, LaRusso NF. Cholangiocyte primary cilia in liver health and disease. *Dev Dyn* 2008;237:2007–12.
- 45 Diener DR, Lupetti P, Rosenbaum JL. Proteomic analysis of isolated ciliary transition zones reveals the presence of ESCRT proteins. *Curr Biol* 2015;25:379–84.
- 46 Ott C, Nachmias D, Adar S, Jarnik M, Sherman S, Birnbaum RY, Lippincott-Schwartz J, Elia N. Vps4 is a dynamic component of the centrosome that regulates centrosome localization of  $\gamma$ -tubulin, centriolar satellite stability and ciliogenesis. *Sci Rep* 2018;8:3353.
- 47 Grati M'hamed, Chakchouk I, Ma Q, Bensaid M, Desmidt A, Turki N, Yan D, Baanannou A, Mittal R, Driss N, Blanton S, Farooq A, Lu Z, Liu XZ, Masmoudi S. A missense mutation in DCDC2 causes human recessive deafness DFNB66, likely by interfering with sensory hair cell and supporting cell cilia length regulation. *Hum Mol Genet* 2015;24:2482–91.
- 48 Meng H, Smith SD, Hager K, Held M, Liu J, Olson RK, Pennington BF, DeFries JC, Gelernter J, O'Reilly-Pol T, Somlo S, Skudlarski P, Shaywitz SE, Shaywitz BA, Marchione K, Wang Y, Paramasivam M, LoTurco JJ, Page GP, Gruen JR. From the cover: DCDC2 is associated with reading disability and modulates neuronal development in the brain. *Proc Natl Acad Sci U S A* 2005;102:17053–8.
- 49 Schumacher J, Anthoni H, Dahdouh F, König IR, Hillmer AM, Kluck N, Manthey M, Plume E, Warnke A, Remschmidt H, Hülsmann J, Cichon S, Lindgren CM, Propping P, Zucchelli M, Ziegler A, Peyrard-Janvid M, Schulte-Körne G, Nöthen MM, Kere J. Strong genetic evidence of DCDC2 as a susceptibility gene for dyslexia. *Am J Hum Genet* 2006;78:52–62.
- 50 Schueler M, Braun DA, Chandrasekar G, Gee HY, Klasson TD, Halbritter J, Bieder A, Porath JD, Airik R, Zhou W, LoTurco JJ, Che A, Otto EA, Böckenhauer D, Sebire NJ, Honzik T, Harris PC, Koon SJ, Gunay-Aygun M, Saunier S, Zeres K, Bruechle NO, Drenth JPH, Pelletier L, Tapia-Páez I, Lifton RP, Giles RH, Kere J, Hildebrandt F. Dcdc2 mutations cause a renal-hepatic ciliopathy by disrupting Wnt signaling. *Am J Hum Genet* 2015;96:81–92.